PROCEEDINGS, 43rd Workshop on Geothermal Reservoir Engineering
Stanford University, Stanford, California, February 12-14, 2018
SGP-TR-213

High-Resolution Seismic Imaging for Geothermal Exploration at Eleven-Mile Canyon in Nevada

Miao Zhang[1], Lianjie Huang[1], Kai Gao[1], Yunsong Huang[1], and Andrew Sabin[2]

[1]Geophysics Group, Los Alamos National Laboratory, Los Alamos, NM 87545, USA

[2]Navy Geothermal Program Office, China Lake, CA 93555, USA

mzhang@lanl.gov; ljh@lanl.gov; kaigao@lanl.gov; yunsongh@lanl.gov; andrew.sabin@navy.mil

Keywords: Anisotropic Reverse-Time Migration, Eleven-Mile Canyon, Fracture Zone, Geothermal Exploration

ABSTRACT

U.S. Navy Geothermal Program acquired seismic data along five lines at Eleven-Mile Canyon in Nevada for geothermal exploration. The data contains significant ground-roll noise and reflection signals are week, resulting in a great challenge to image subsurface structures. We successfully remove the ground-roll noise using our newly developed wavenumber-adaptive frequency-space filtering technique. We then build anisotropic models along the five lines using anisotropic full-waveform inversion of the seismic data. Finally, we perform anisotropic reverse-time migration using the anisotropic models and our newly processed seismic data to obtain high-resolution subsurface images at Eleven-Mile Canyon. Our anisotropic full-waveform inversion and anisotropic reverse-time migration provide high-resolution images at Eleven-Mile Canyon, and these images could be useful for geothermal exploration in combination with imaging results of other geophysical data.

1. INTRODUCTION

The Eleven-Mile Canyon geothermal exploration field is located near the margins of Dixie Valley, a NNE-SSW-trending late Cenozoic structural basin, 100 kilometers east of Fallon, Nevada. It is close to the surface rupture terminations of 1954 Fairview Peak – Dixie Valley earthquake sequence (Caskey et al., 1996). The Hunt Energy Corporation initially discovered the Eleven-Mile Canyon geothermal system through a wildcat drilling operation in the late 1970's. Geothermal exploration was halted after Hunt Energy Corporation filed for bankruptcy. In 1999, the U.S. Navy acquired portions of these lands as part of a land withdrawal for the Naval Air Station Fallon (NASF) electronic warfare training range and exploration was subsequently resumed by the Navy Geothermal Program Office (GPO) in 2005 (Alm et al., 2016; Unruh et al., 2016). In 2013, Navy GPO conducted five 2D seismic surveys to evaluate geothermal potential at Eleven-Mile Canyon. Lines 1, 2, 3, and 4 are along west-east direction to cross the valley (Fig. 1). Line 5 is in a north-south direction that intersects Lines 1, 2, and 3 (Fig. 1), so that horizon and fault interpretations can be made with greater confidence between independent lines.

Eleven-Mile Canyon locates in the Basin and Range province and it belongs to "typical" basin and range geothermal systems (Blackwell et al., 2012). Eleven-Mile Canyon geothermal exploration site contains a complex network of faults and fractures with steep dips. It is crucial to image and delineate subsurface fracture/fault zones for geothermal exploration because fracture/fault zones may provide paths for hydrothermal flow, or they may be effective barriers to geothermal flow in some situations (Ba et al., 2015). It is particularly challenging to image fracture zones because of complicated heterogeneities and anisotropic properties in fracture zones and surrounding rocks.

Reverse-time migration (RTM) is one of the most powerful tools for imaging complex subsurface structures. RTM solves the wave equation for wavefield extrapolation and can handle complex subsurface structures. Conventional RTM using the isotropic assumption is not always appropriate because of the existence of seismic anisotropy in the subsurface, especially in complex geothermal field (Gao and Huang, 2015). In anisotropic media, conventional isotropic wave propagation assumption can result in misplaced images of reflectors, image artifacts, and low image resolution (Zhan et al., 2012). Therefore, fracture/fault zones could be wrongly positioned or totally missing when using conventional RTM based on the isotropic assumption for subsurface imaging. By assuming the weak anisotropy of subsurface media, the acoustic approximation has been used to describe the anisotropy using Thomsen parameters and reference velocity values (Thomsen, 1986; Plessix and Cao, 2011).

We develop an anisotropic acoustic reverse-time migration method (anisotropic RTM) based on the Thomsen parameters. The method uses an implicit wavefield separation scheme to improve migration imaging. We verify the effectiveness of our anisotropic acoustic RTM method using synthetic data for a "typical" basin and range geothermal model by comparing our imaging results with those obtained using the conventional isotropic RTM. We use an optimized correlation-based anisotropic full-waveform inversion method to invert velocity models and Thomsen parameters. Then we apply our anisotropic RTM to the five 2D lines of surface seismic reflection data acquired at Eleven-Mile Canyon, and compare our images with those obtained using industry Kirchhoff migration.

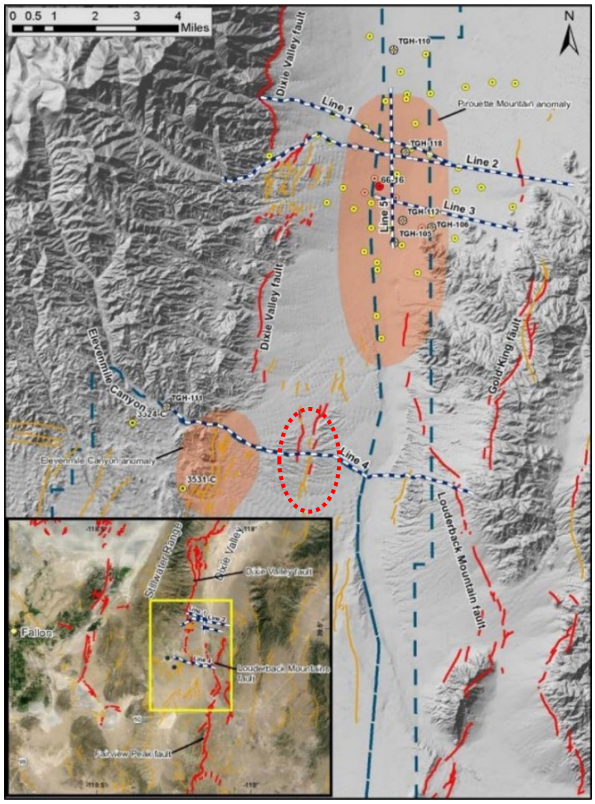

Figure 1: Location map of the Eleven-Mile Canyon geothermal exploration site in southern Dixie Valley, with five 2-D seismic survey lines along the white dashed lines. Faults shown are from the U.S. Geological Survey Quaternary fault and fold database. Orange indicates late Quaternary activity; red zones indicate area of surface rupture during the 1954 earthquake sequence; dashed red ellipse suggests the corresponding identified fault in Line 4 as indicated in Figure 6 (Unruh et al., 2016).

2. ANISOTROPIC RESERVE-TIME MIGRATION

Conventional isotropic reverse-time migration (RTM) methods can lead to incorrectly positioned or missed images of reflectors in anisotropic media. However, fracture zones/faults and subsurface geologic layers in geothermal exploration sites usually behave as anisotropic media. To improve subsurface imaging for geothermal exploration, we implement anisotropic acoustic reverse-time migration using a wavefield separation imaging condition.

Conventional modeling and migration for tilted transversely isotropic (TTI) media may suffer from numerical instabilities and shear wave artifacts because of the coupling of the P-wave and SV-wave modes in the TTI coupled equations. We adopt the decoupled P-wave equations in the time-wavenumber domain for 2D TTI media (Zhan et al. 2012):

$$\frac{1}{V_{P_0}^2}\frac{\partial^2 P}{\partial t^2} = -\left\{ \begin{array}{l} k_x^2 + k_z^2 \\ +(2\varepsilon\cos^4\theta + 2\delta\sin^2\theta\cos^2\theta)\dfrac{k_x^4}{k_x^2+k_z^2} + (2\varepsilon\sin^4\theta + 2\delta\sin^2\theta\cos^2\theta)\dfrac{k_z^4}{k_x^2+k_z^2} \\ +(-4\varepsilon\sin 2\theta\cos^2\theta + \delta\sin 4\theta)\dfrac{k_x^3 k_z}{k_x^2+k_z^2} + (3\varepsilon\sin^2 2\theta - \delta\sin^2 2\theta + 2\delta\cos^2 2\theta)\dfrac{k_x^2 k_z^2}{k_x^2+k_z^2} \end{array} \right\} P, \quad (1)$$

where V_{P_0} is vertical isotropic P velocity; k_x and k_z are spatial wavenumbers in x and z directions, respectively; ε, δ and θ are Thomsen parameters.

The migration imaging condition is based on the wavefield cross-correlation of forward propagation from a source and backward propagation from receivers. Forward and backward propagation wavefields in RTM contain both upgoing- and dowgoing-wavefileds, which would result in low-frequency migration artifacts. To remove these false images, we apply a fully automatic and computationally efficient de-primary RTM technology developed by Fei et al. 2015. We decompose the source and receiver wavefileds into their directional components, including up and down, and left and right directions (Fei et al., 2015):

$$I_{\text{pp,down}}(\mathbf{x}) = \sum_{N_s,N_r} \int_0^T [P_s P_r - H_z(P_s)H_z(P_r) - P_s H_z(H_t(P_r)) - H_z(P_s)H_t(P_r)]dt, \quad (2)$$

$$I_{\text{pp,left}}(\mathrm{x}) = \sum_{N_s,N_r} \int_0^T [P_s P_r - H_x(P_s)H_x(P_r) + P_s H_x(H_t(P_r)) + H_x(P_s)H_t(P_r)]dt, \quad (3)$$

$$I_{\text{pp,right}}(\mathrm{x}) = \sum_{N_s,N_r} \int_0^T [P_s P_r - H_x(P_s)H_x(P_r) - P_s H_x(H_t(P_r)) - H_x(P_s)H_t(P_r)]dt, \quad (4)$$

where *s* and *r* represent the source and receiver, P is the separated qP-wavefield, H_x, H_z and H_t represent the Hilbert transform in the horizontal direction, vertical direction and time domain.

3. SYNTHETIC TESTS

We apply our anisotropic RTM method to synthetic seismic data generated for a "typical" basin and range geothermal model. The model contains several geological sedimentary layers and several fault zones. Fault zones are from offset between different geological layers. We assume that wave propagation along the horizontal direction is 10%~20% faster than that along the vertical direction. For simplification, we assume it is elliptical anisotropy (e.g., epsilon equals to delta) and theta is associated with orientation of fault zone. Therefore, the constructed fault zones behave as tilted transverse isotropic (TTI) media. We generate synthetic surface seismic reflection data using isotropic Vp model (Fig. 2a) together with these anisotropic parameters. We conduct conventional isotropic RTM using the isotropic Vp model and perform anisotropic RTM using anisotropic models, respectively. The image produced using the conventional RTM is blurred and unfocused, because a single isotropic velocity model cannot provide correct and sufficient kinetic information for anisotropic wavefield propagation (Fig. 2b). By contrast, our anisotropic RTM clearly image these fault zones (Fig. 2c). These synthetic test results demonstrate that our new anisotropic RTM method produces higher-quality images of fracture zones than the conventional isotropic RTM.

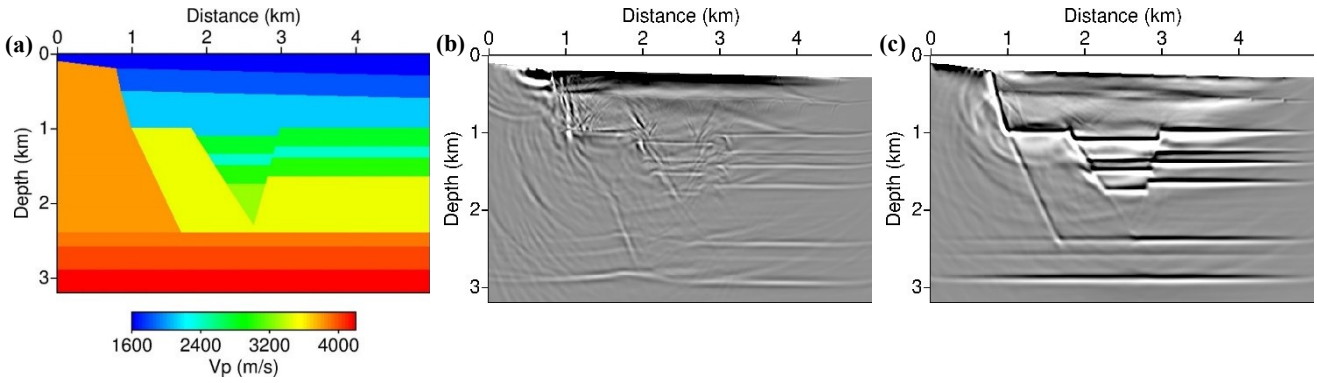

Figure 2: (a) Isotropic P velocity for a "typical" basin and range geothermal model; (b) image obtained using isotropic reverse-time migration; (c) image obtained using anisotropic reverse-time migration.

4. APPLICATION TO SEISMIC DATA FROM ELEVEN-MILE CANYON

We apply anisotropic RTM to the five 2D lines of surface seismic data acquired at Eleven-Mile Canyon in 2013. We assume that the subsurface media contains weak anisotropy described using Thomsen parameters. Only the vertical component of seismic data was acquired in the seismic reflection survey at Eleven-Mile Canyon. We first remove dead traces from the original data, bandpass filter high-frequency noise and balance seismic datum amplitudes. Then we correct their phase and amplitude from 3D to 2D caused by different geometrical spreading. We also use our recently developed wavenumber-adaptive bandpass filter method (Huang et al., 2017) to suppress the ground-roll noise in the seismic data. The initial velocity models are obtained using tomography inversion of first-arrival traveltimes. We update the velocity model and anisotropic parameters using an optimized correlation-based full-waveform inversion method (Choi et al., 2016).

We briefly summarize these procedures as below:

1) Process the raw seismic data for each seismic line;
2) Update isotropic Vp using full-waveform inversion (FWI) and initial velocity model obtained using refraction tomography;
3) Estimate the initial theta parameter from reverse-time migration image;
4) Invert anisotropic models ($V_{P_0}, \varepsilon, \delta$ and θ) using anisotropic FWI together with the updated isotropic Vp and estimated theta;
5) Image subsurface structures using anisotropic reverse-time migration and inverted anisotropic models.

Figures 3-7 show the image comparisons between the industry Kirchhoff migration images and our anisotropic RTM images. Our anisotropic RTM yields more clear and continuous images compared to those obtained using industry Kirchhoff migration. We observe the east- and west-dipping structures in Lines 1, 2, 3 and 4, which intersect north-south-dipping structures (Line 5) and are consistent with local geological structure. A fault zone can be seen at ~5.3 km in Line 4, which corresponds to a mapped fault in U.S. Geological Survey (USGS) fault database shown in Fig. 1.

Figures 8-10 show intersected image comparisons of different independent lines. The intersected images produced using our anisotropic RTM are consistent at the intersections of different lines in 3D space. However, we cannot find these expected consistencies from the industry Kirchhoff migration images. These consistencies in 3D space is a clear evidence that the images obtained using our anisotropic RTM are more accurate and reliable compared to the industry Kirchhoff migration images.

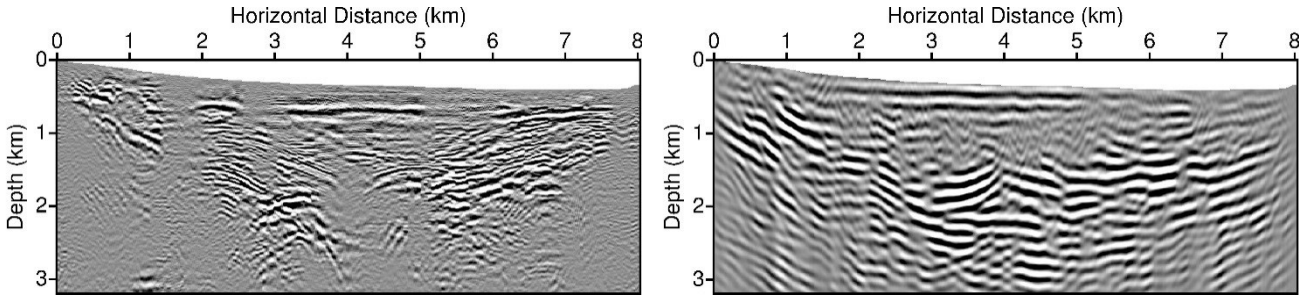

(a) Industry Kirchhoff migration image **(b) LANL's anisotropic RTM image**

Figure 3: Comparison between industry Kirchhoff migration image (a) and our anisotropic RTM image (b) for seismic data in Line 1.

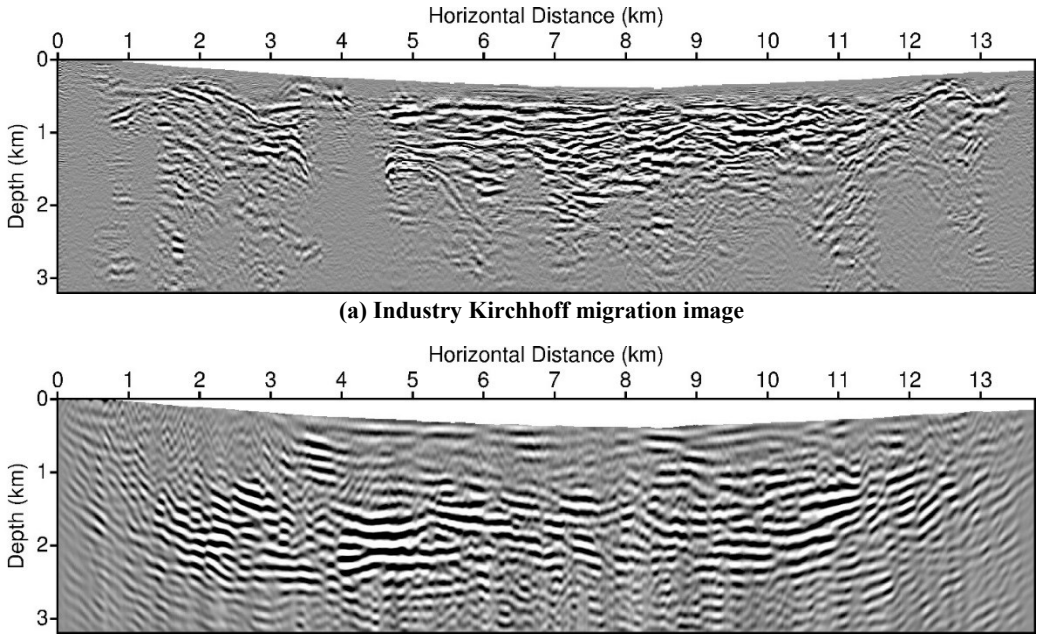

(a) Industry Kirchhoff migration image

(b) LANL's anisotropic RTM image

Figure 4: Comparison between industry Kirchhoff migration image (a) and our anisotropic RTM image (b) for seismic data in Line 2.

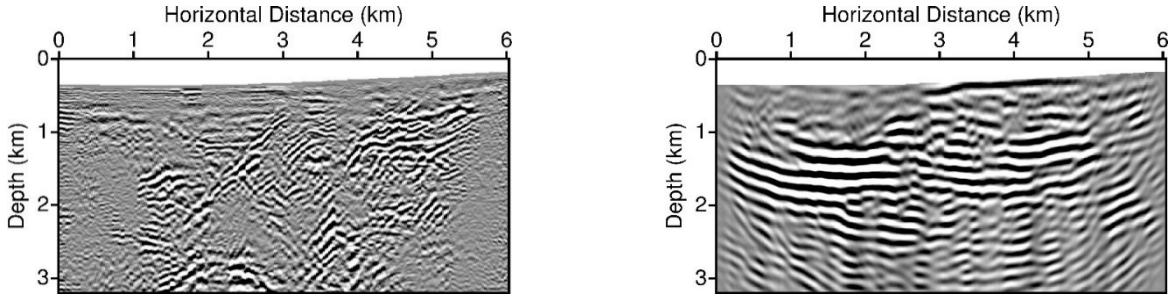

(a) Industry Kirchhoff migration image **(b) LANL's anisotropic RTM image**

Figure 5: Comparison between industry Kirchhoff migration image (a) and our anisotropic RTM image (b) for seismic data in Line 3.

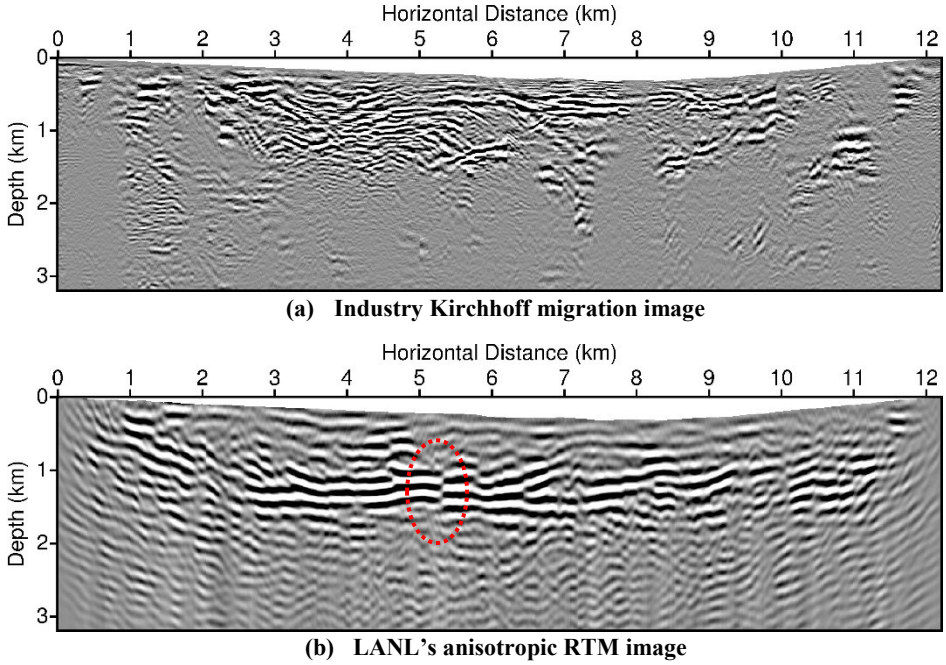

(a) Industry Kirchhoff migration image

(b) LANL's anisotropic RTM image

Figure 6: Comparison between industry Kirchhoff migration image (a) and our anisotropic RTM image (b) for seismic data in Line 4. The fault within the dashed red ellipse is consistent with a mapped fault in Figure 1.

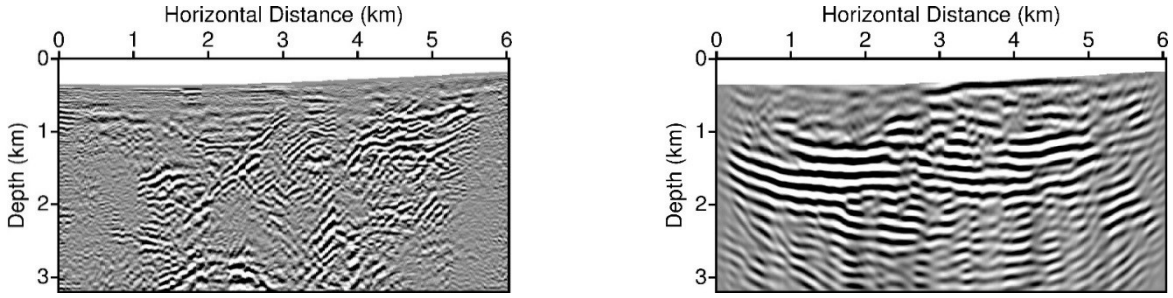

(a) Industry Kirchhoff migration image **(b) LANL's anisotropic RTM image**

Figure 7: Comparison between industry Kirchhoff migration image (a) and our anisotropic RTM image (b) for seismic data in Line 5.

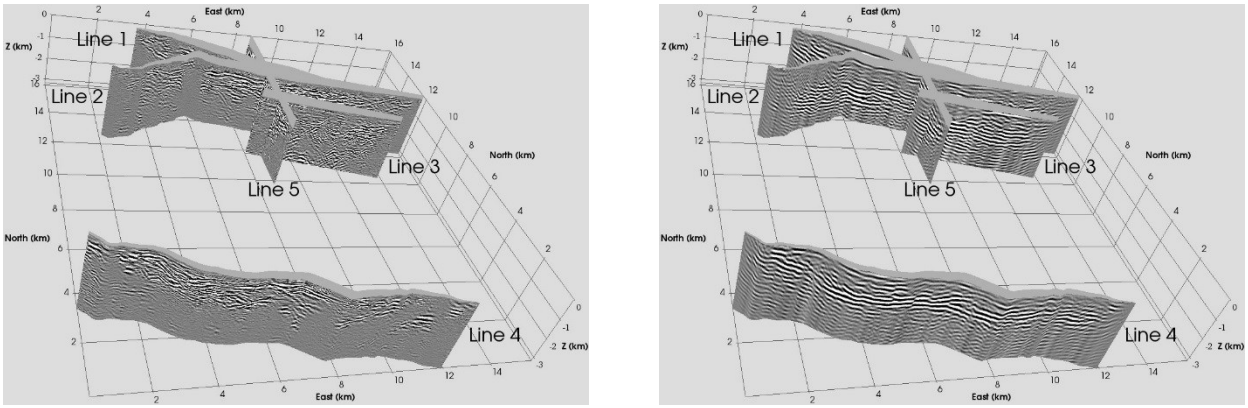

(a) Industry Kirchhoff migration image **(b) LANL's anisotropic RTM image**

Figure 8: 3D overview of industry Kirchhoff migration images (a) and our anisotropic RTM images (b).

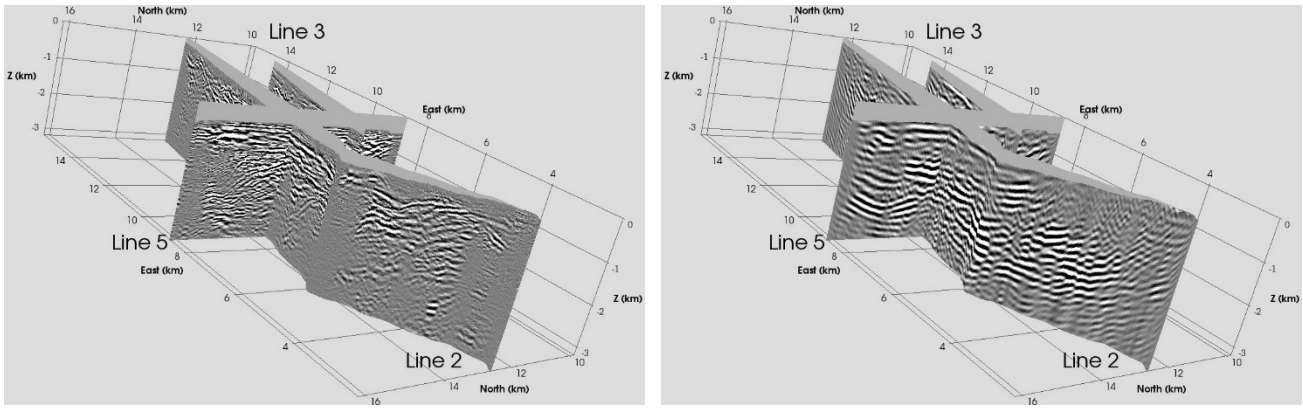

(a) Industry Kirchhoff migration image **(b) LANL's anisotropic RTM image**

Figure 9: North-West 3D view of industry Kirchhoff migration images (a) and our anisotropic RTM images (b).

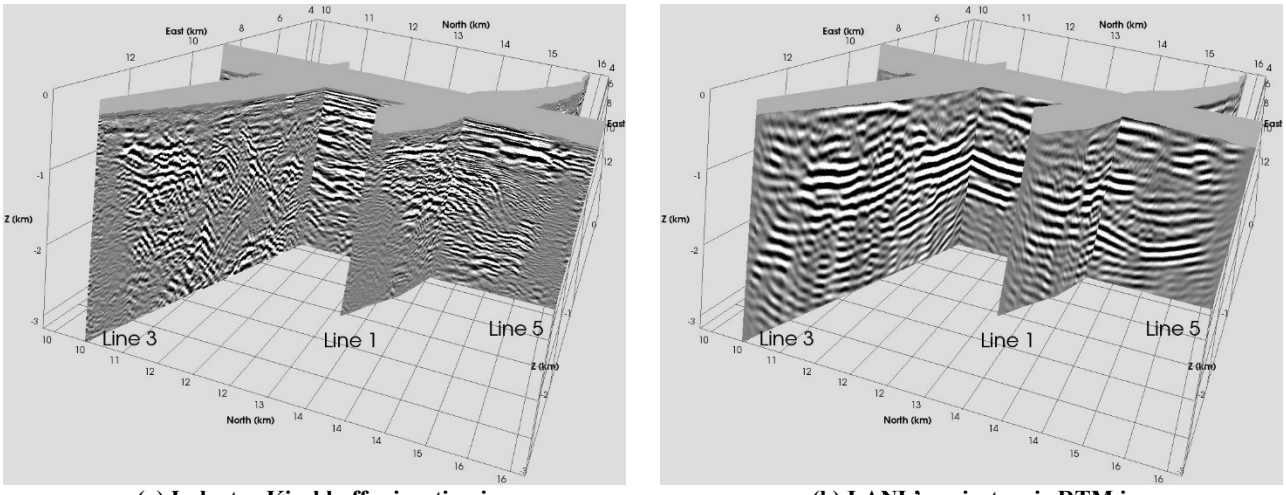

(a) Industry Kirchhoff migration image **(b) LANL's anisotropic RTM image**

Figure 10: North-East 3D view of industry Kirchhoff migration images (a) and our anisotropic RTM images (b).

5. CONCLUSIONS

We have developed and verified a new anisotropic acoustic reverse-time migration method using synthetic seismic data for a "typical" basin and range geothermal model. The model contains several fault zones with anisotropic properties. Our anisotropic reverse-time migration produces clear images of fault zones and much fewer image artifacts. We have applied our anisotropic acoustic reverse-time migration method to the five 2D lines of seismic data acquired at Eleven-Mile Canyon. Our anisotropic reverse-time migration significantly improves the quality and resolution of subsurface images in Eleven-Mile Canyon. Our anisotropic reverse-time migration images can be merged coherently one another along different 2D survey lines, but the industry Kirchhoff migration images cannot. Our results demonstrate that it is essential to properly accounting for anisotropic properties for reliable imaging of subsurface complex structures including fault/fracture zones for geothermal energy exploration.

6. ACKNOWLEDGEMENTS

This work was supported by the Geothermal Technologies Office (GTO) of the U.S. Department of Energy through contract DE-AC52-06NA25396 to Los Alamos National Laboratory (LANL). The computation was performed using super-computers of LANL's Institutional Computing Program.

REFERENCES

Alm, A., Walker, J. D., and Blake, K.: Structural Complexity of the Pirouette Mountain and Elevenmile Canyon Geothermal Systems, *Transactions, Geothermal Resources Council*, **40**, (2016), 433-438.

Ba, J., Du, Q., Carcione, J.M., Zhang, H., and Muller, T.M.: Seismic exploration of hydrocarbons in heterogeneous reservoirs, first ed.: Elsevier (2015).

Blackwell, D., Waibel, A. F., and Richards, M.: Why Basin and Range Systems Are Hard to Find: The Moral of the Story is They Get Smaller With Depth, *Transactions, Geothermal Resources Council*, **36**, (2012), 1321-1326.

Caskey, S. J., Wesnousky, S. G., Zhang, P., and Slemmons, D. B.: Surface faulting of the 1954 Fairview Peak (MS 7.2) and Dixie Valley (MS 6.8) earthquakes, central Nevada, *Bulletin of the Seismological Society of America*, **86**, (1996), 761-787.

Choi, Y., and Alkhalifah, T.: An Optimized Correlation-based Full Waveform Inversion, *78th EAGE Conference and Exhibition* 2016, Vienna, Austria (2016).

Fei, T., Luo, Y., Yang, J., Liu H., and Qin, F.: Removing false images in reverse time migration: The concept of de-primary, *Geophysics*, **80**(5), S237-S244.

Gao, K., and Huang, L.: Anisotropic Elastic-Waveform Modeling for Fracture Characterization in EGS Reservoirs, *Proceedings,* 40th Workshop on Geothermal Reservoir Engineering, Stanford University, Stanford, CA (2015).

Huang, Y., Zhang, M., and Huang, L.: Ground-roll noise suppression in land surface seismic data using a wavenumber-adaptive bandpass filter, *Transactions, Geothermal Resources Council*, **41**, (2017), 1659-1668.

Plessix, R.E., and Cao, Q.: A parametrization study for surface seismic full waveform inversion in an acoustic vertical transversely isotropic medium, *Geophysical Journal International*, **185**, (2011), 539-556.

Thomsen, L.: Weak elastic anisotropy, *Geophysics*, **51**, (1986), 1954-1966.

Unruh, J., Gray, B., Christopherson, K., Pullammanappallil, S., Alm, S., and Blake, K.: Seismic Reflection and Magnetotelluric Imaging of Southwestern Dixie Valley Basin, Nevada, *Transactions, Geothermal Resources Council*, **40**, (2016), 455-461.

Zhan, G., Pestana, R. C., and Stoffa, P. L.: Decoupled equations for reverse time migration in tilted transversely isotropic media, *Geophysics*, **77**, (2012), T37-T45.